

PCCP

Accepted Manuscript



This is an *Accepted Manuscript*, which has been through the Royal Society of Chemistry peer review process and has been accepted for publication.

Accepted Manuscripts are published online shortly after acceptance, before technical editing, formatting and proof reading. Using this free service, authors can make their results available to the community, in citable form, before we publish the edited article. We will replace this *Accepted Manuscript* with the edited and formatted *Advance Article* as soon as it is available.

You can find more information about *Accepted Manuscripts* in the [Information for Authors](#).

Please note that technical editing may introduce minor changes to the text and/or graphics, which may alter content. The journal's standard [Terms & Conditions](#) and the [Ethical guidelines](#) still apply. In no event shall the Royal Society of Chemistry be held responsible for any errors or omissions in this *Accepted Manuscript* or any consequences arising from the use of any information it contains.



Cite this: DOI: 10.1039/xxxxxxxxxx

Fundamental Aspects in Surface Self-Assembly: A Theoretical Study of Polarity and Shape[†]

Emilian Tuca^a and Irina Paci^{*a}Received Date
Accepted Date

DOI: 10.1039/xxxxxxxxxx

www.rsc.org/journalname

We investigate fundamental aspects of structure formation in molecular self-assembly, by examining the emergence of order upon adsorption of a series of model molecules. It is known that strongly polar diatomic molecules form three-dimensional crystals in the absence of a substrate. This tendency can be disrupted upon assembly on a solid surface, and various other types of order may arise. Depending on the relative strength of the interactions, disordered phases, two-dimensional crystals commensurate to the surface, and unmodified crystals were observed upon adsorption of simple dipoles in the present work. Introduction of steric features, in the form of a longer backbone or substituents external to the polar pair, led to even richer phase diagrams. The formation of two-dimensional phases with nematic (parallel) or antiparallel alignment was accomplished by altering the polarity of the end groups on needle-like molecules, whereas embedded charged groups made two-dimensional structure unstable for even very long molecules. These molecules preferred to align in long, often desorbed, molecular wires. The wealth of phases observed here parallel the results of experimental systematic or incidental studies of the relationships between molecular interactions and self-assembled patterns, and provide some insight into the molecular handles that self-assembly researchers can wield to guide the process towards a desired structural outcome.

1 Introduction

The field of surface self-assembly has received significant attention in the past two decades, as a result of improved experimental techniques and a growing interest in device miniaturization and the fabrication of organic functional materials. Molecular SA is the spontaneous aggregation of molecules into structured, stable, non-covalently joined aggregates under equilibrium conditions.¹ It has been seen as a promising approach to manufacturing materials with desired functionalities, by designing appropriate building blocks and controlling the assembly environment.^{2,3} Within the broad field of molecular SA, self-assembly on surfaces is of particular interest due to its applications in surface protection,^{4,5} fabrication of nanoscale devices,⁶ dip-pen nanolithography,^{7,8} solar cells,⁹ biosensor production,¹⁰ and chiral separation.^{11,12}

Despite significant effort^{13–15} towards the development of guiding principles, both general and specific, in molecular and surface SA, much is still left to understand. Theoretical ap-

proaches have attempted to unravel this complex phenomenon by individually addressing distinct length and time scales, using different levels of theory.¹⁶ One of the most well-studied SA systems are monolayers of normal alkanethiolates, which balance functionality with highly reproducible behavior and have been useful for studying basic aspects of SA.^{17–19} These include the behavior of tilt angles, side chain effects, the importance of the main chain length, with longer chains yielding more stable SAMs, and the odd-even effect, where the addition of one carbon atom in the chain can dramatically alter SA patterning.^{20,21} These effects and behaviors have already been exploited in applications such as surface protection^{4,5} and functionalization.^{22–31}

Substitution of alkanethiol tails can influence and even direct SA,^{17,32,33} to control molecular surface area, phase stability, as well as the chemical and physical behavior of the surface.^{23,25,28,30,32,34,35} One example is the fabrication of molecular switches,^{36–38} where the molecule or assembly has the ability to adopt one of two or more distinct phases in the presence of an external stimulus. Whereas thiolate backbones can form stable SAMs by close packing, this can destabilize one of the two phases and inhibit the switching process.³⁹ In such cases, the preparation of the monolayer in the in the less dense phase is required for the proper functioning of the switch.⁴⁰ On the other hand, weaker lateral interactions in the low-density monolayer can lead

^a Department of Chemistry and the Centre for Advanced Materials and Related Technology, University of Victoria, Victoria, BC, V8W 3V6, Canada; Tel: 1 250 472 4946; E-mail: ipaci@uvic.ca

[†] Electronic Supplementary Information (ESI) available: [Snapshots and graphics regarding: system size convergence; variation of order parameters and standard deviations; further data on longer tails for model G variations; further data on the fraction of molecules touching the surface]. See DOI: 10.1039/b000000x/

to enhanced configurational freedom and a higher degree of disorder in the molecular backbones. In short, attaining a balance between molecular flexibility and structural stability is a fundamental aspect of molecular engineering. One way to achieve this balance is by considering the fundamental forces that drive SA at the molecular level.

Many of the basic features of alkythiol SAMs were also observed in other molecular systems. Experimental work revealed SA patterns ranging from one-dimensional arrays^{41–43} to cyclic networks,¹⁴ to pentagonal and hexagonal aggregates.^{1,44–47} The specifics differ from case to case, but a few factors appear to be essential in determining the outcomes of surface patterning: the size and shape of building blocks, the surface geometry and its geometric compatibility with the adsorbate, and intermolecular interactions. The latter are often a combination of dispersive effects from alkythiol chains, π -stacking interactions and molecular dipole moments created by polar groups and heteroatoms. All these properties are tools that could potentially be used to direct the SA process, provided a thorough understanding of the underlying chemistry and physics is developed. The greatest challenge in this comes from the complexity with which the many variables interact with one another in any particular system. Given the subtle interplay of intermolecular forces, relatively simple systems, such as small organic molecules on metal surfaces, can give rise to unpredictable patterns. A change in one parameter of the system, such as the symmetry of the surface, the position of a functional group, or annealing temperature, can have a dramatic effect on SA.

One approach to tackling this complexity at a fundamental level is by examining the various contributions to the free energy of self-assembly, using statistical approaches.^{15,48–50} Distinct formalisms have been developed for supramolecular and block copolymer bulk self-assembly,¹⁵ as well as surface-bound molecules.⁵⁰ Thermodynamic and kinetic aspects of the process have been examined in an approximative or qualitative fashion, including the role of entropy,^{15,51} polymorphism,⁵¹ pair interactions⁵⁰ and cooperativity.^{52,53} Molecular features were described using approximate partition functions and equilibrium constants,^{50,54} and parallels were drawn to instances where designed self-assembly was achieved experimentally.^{15,51} These studies have made significant inroads in the formal understanding of self-assembly processes, at a qualitative or semiquantitative level, but research still has to bridge the length and complexity scales between this level of theory and the variable space in which experiments take place.

Molecular modeling of systems of ever-increasing complexity are an attempt to bridge this gap. In simple model systems, the variable space that a given system exists in is reduced, and the outcome of the self-assembly process can often be traced directly to its structural or interactional causes. Here, we use a series of molecular models to investigate how the competition between dipole-dipole interaction and steric/geometric effects gives rise to a variety of surface assembly patterning on surface. These interactions are in a sense a first-order approximation for surface SA, since these are the minimum requirements for ordered phase formation. By tuning the molecular and surface parameters in

systems comprised of multiple two- to six-atom molecules and a substrate, we attempt to understand how the interplay of these parameters gives rise to complex equilibrium patterning.

2 Methods and Models

2.1 Parallel Tempering Monte Carlo (PTMC) in the Canonical Ensemble

When dealing with systems evolving on complicated potential energy surfaces (PESs), the main problem is entrapment in local minima, an undesirable effect when aiming for thermodynamic control. The problem manifests particularly at low temperatures and high densities, and is addressed experimentally by preparation methods such as repeated annealing. In simulations, several options are available to overcome trapping on complex PESs. One such methodology is the parallel tempering algorithm, which has radically improved sampling in the Metropolis MC methodology.^{55–58} The method involves simulations of several copies, or replicas, of the system, each evolving in a distinct thermodynamic state (at different temperatures, for example). Occasionally, a swap of configurations between two replicas is performed. The parallel tempering formalism is thus a Markov chain consisting of two types of moves: standard MC moves, where the configuration of a given replica is changed randomly, with acceptance probabilities given by the Metropolis criterion, and swap moves between two distinct replicas of the system, i and j , where i is selected at random and normally $j = i + 1$. Swaps between replicas that are in similar thermodynamic states have higher acceptance probabilities. In temperature-based PTMC, the temperature grid is determined either automatically or manually, by the overlap of the energy histograms corresponding to pairs of neighboring replicas. After an equilibration interval, in which the state of the system depends on the starting configuration, sampling in each replica becomes representative of equilibrium behavior in that thermodynamic state.

2.2 Models and potentials

In the present work, molecular models were designed to interact through a Lennard-Jones-electrostatic (LJe) potential, in a simulation box containing a surface. The LJe potential is given by

$$U_{ab} = \sum_{i,j=1}^{n_{at}} \left[4\epsilon_{ij} \left(\left(\frac{\sigma_{ij}}{r_{ij}} \right)^{12} - \left(\frac{\sigma_{ij}}{r_{ij}} \right)^6 \right) + \frac{q_i q_j e^2}{4\pi\epsilon_0 r_{ij}} \right] \quad (1)$$

where a and b are the two interacting molecules and n_{at} is the number of atoms in a given molecule. The LJ energy parameter ϵ_{ij} is the depth of the potential energy well, and σ_{ij} is the finite distance at which the potential is zero. r_{ij} is the distance between the two atoms, q_i is the partial charge on atom i , e is the electrostatic charge and ϵ_0 is the dielectric constant of vacuum. Mixed Lennard-Jones parameters were obtained using the Lorentz-Berthelot mixing rules: $\sigma_{ij} = (\sigma_{ii} + \sigma_{jj})/2$, and $\epsilon_{ij} = \sqrt{\epsilon_{ii}\epsilon_{jj}}$. All molecules and the surface were rigid, i.e. all bond lengths, bond angles and torsion angles were held fixed, and no surface atom vibration or surface reconstruction were allowed.

2.3 Model description and naming

To understand how electrostatic interactions compete with surface potential and steric/geometric factors to give rise to specific patterns, we investigated five series of models, as shown in Figure 1. All models possessed a dipole moment created by a pair of atoms which had equal and opposite charges but were otherwise identical.

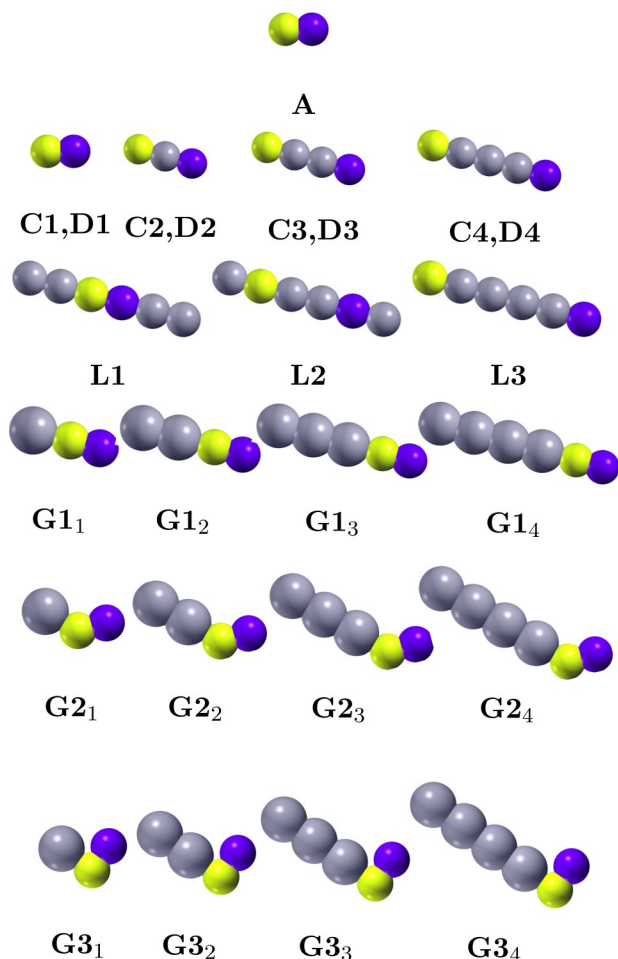


Fig. 1 Models used, with the atoms carrying partial charges highlighted in yellow and purple. Grey atoms carried no charge. Symbols are determined by the effect they help study.

Series A (basic), a series of simple diatomic dipolar models, was used to investigate the competition between intermolecular interaction strengths and surface potentials. Steric effects were added in series C (constant Charge), comprised of molecules with charged end atoms, with constant charges and different molecular lengths (see Figure 1). Altering charge separation changes dipoles however, so series D (constant Dipole), with constant dipole moments but varying molecular lengths was additionally considered. In series D, the dipole moment was held constant by lowering atomic charges as charge separation increased. Molecules in series L (constant Length) also exhibited constant dipole moments, with varying dipolar lengths and charges, within overall constant molecular lengths. Finally, set G_N (for Geometric

effects) was formed of molecules with two charged atoms and N neutral atoms, and varying bond angles.

Interaction parameters for the different model series are presented in Table 1. Note that reduced units are used throughout, and the results discussed below are valid for an infinite number of systems, due to the law of corresponding states. One such state, for the system with $\sigma_{11} = 3.65 \text{ \AA}$ and $\epsilon_{11} = 0.9 \text{ kJ/mol}$, has $T^* = 1$ corresponding to a temperature of 204 K. The interaction of a methyl group in an alkane with a graphite surface would correspond to a $\sigma_{11} = 3.95 \text{ \AA}$ and a $\sigma_{ss} = 3.55 \text{ \AA}$.⁵⁹ Given the $\epsilon_{11} \approx \epsilon_{ss} = 1.23 \text{ kJ/mol}$, $T^* = 1$ in this system corresponds to a temperature of 148 K. On the other hand, for methanethiol/gold system, a back-of-the-envelope calculation shows the dipole-dipole contribution to lateral interactions to be roughly 5 times smaller than the molecule-surface interaction. This corresponds in the present work to an A1-like model with $\epsilon_{ss} = 1$ and charges of 0.08 of an electron.

Table 1 Interaction parameters for the investigated models

Model*	n_{at}	q^{\parallel}	$\sigma_{ii}^* (\epsilon_{ii}^*)^{\ddagger}$	$\sigma_{ss}^* (\epsilon_{ss}^*)^{\ddagger}$
A1	2	0.01	1 (1)	1 (1; 3 [§])
A2	2	0.10	1 (1)	1 (1; 3 [§])
A3	2	0.20	1 (1)	1 (1; 3 [§])
C1- <i>l</i>	2	0.05	1 (1)	1 (1.5)
C2- <i>l</i>	3	0.05	1 (1)	1 (1.5)
C3- <i>l</i>	4	0.05	1 (1)	1 (1.5)
C4- <i>l</i>	5	0.05	1 (1)	1 (1.5)
C1- <i>h</i>	2	0.20	1 (1)	1 (1.5)
C2- <i>h</i>	3	0.20	1 (1)	1 (1.5)
C3- <i>h</i>	4	0.20	1 (1)	1 (1.5)
C4- <i>h</i>	5	0.20	1 (1)	1 (1.5)
D1	2	0.20	1 (1)	1 (1.5)
D2	3	0.10	1 (1)	1 (1.5)
D3	4	0.07	1 (1)	1 (1.5)
D4	5	0.05	1 (1)	1 (1.5)
L1	6	0.20	1 (1)	1 (1.5)
L2	6	0.07	1 (1)	1 (1.5)
L3	6	0.04	1 (1)	1 (1.5)
G1- <i>l</i>	3	0.05	1 [¶] (1)	1 (1.5)
G2- <i>l</i>	3	0.05	1 (1)	1 (1.5)
G3- <i>l</i>	3	0.05	1 (1)	1 (1.5)
G1- <i>h</i>	3	0.20	1 (1)	1 (1.5)
G2- <i>h</i>	3	0.20	1 (1)	1 (1.5)
G3- <i>h</i>	3	0.20	1 (1)	1 (1.5)

*The *-h* and *-l* notation was used to denote the high charge and low charge versions of models C and G.

[¶]In each molecule, one atom has $+q$ charge and another atom has a $-q$ charge (See Figure 1). q is given in fractions of one electronic charge.

[‡]Reduced LJ parameters are relative to the charged atom LJ parameters. The ϵ parameter is given in brackets. The *s* subscript refers to surface parameters, while *i* refers to atoms in the adsorbate.

[§]Two different values of the reduced surface-molecule interaction parameters were used.

[¶]In the G-series molecules, all uncharged atoms had a larger σ^* (= 1.2).

2.4 Numerical details and surface model

Each simulation followed either 80 (in simulations of models C, D, L and G) or 100 (models A) molecules, using a PTMC procedure over a range of temperatures. Preliminary calculations for models A and C with 30, 50, 80 and 100 molecules indicated a switch between edge-driven properties and bulk-driven properties around 50 molecules (see ESI Figure 1†, for example). Two square surface layers were considered from the (100) facet of the FCC crystal, totaling 1156 atoms (for a simulation box length of 25 reduced units). Box sizes were chosen such that a low density two-dimensional phase was created, and condensed patterns were not affected by variation of box size. Periodic boundary conditions were found to have no impact on simulation outcomes in these circumstances, and were not employed in any of the reported results. Evaporative events (particles leaving the simulation box) were forbidden, by rejecting moves that lead to evaporation.

Preliminary calculations using slightly larger ($\sigma_s = 1.2$) surface atoms and (111) facets produced results qualitatively similar to those reported here, with ($\sigma_s = 1.2$) and (100) facet. The change in surface atom density, whether by larger surface atoms or by a more compact (111) layout, was reflected mainly in the increase of overall surface-molecule interaction strengths, and was qualitatively equivalent to an increase in the surface potential parameter. This mirrored our previous experience with purely dispersive substrates.^{55,60} In consequence, the results presented below were obtained with a (100) substrate.

Simulations were run for at least 10^9 MC steps, until structural and energy convergence was observed. Averages were collected post-equilibration over another 10^9 MC steps. The temperature range was, in all cases, large enough to sample the configurational space thoroughly, with the highest temperature always leading to gaseous phase. Between 35 and 70 replicas were necessary for the various systems, with attempted swaps performed in 5% of the moves. The target acceptance ratio for temperature swaps was 10%, and the number and spacing of replicas was adjusted to attempt to meet it. As a rule, systems with a sharper potential energy surface (created by stronger electrostatic potentials) required larger numbers of replicas to equilibrate.

2.5 Order Parameters

To investigate the degree of order in the systems, three order parameters, S_1 , S_2 and S_4 were chosen. These are statistical quantities given by:

$$\begin{aligned} S_1 &= \langle \cos \theta_{ij} \rangle \\ S_2 &= \frac{\langle 3 \cos^2 \theta_{ij} - 1 \rangle}{2} \\ S_4 &= \frac{\langle 35 \cos^4 \theta_{ij} - 30 \cos^2 \theta_{ij} + 3 \rangle}{8} \end{aligned} \quad (2)$$

where θ_{ij} is the angle between the dipoles of molecule i and j and averaging is performed over all distinct pairs of molecules in the system, then over MC steps. The quantities S_1 , S_2 and S_4

can vary between 0 and 1 and are measures of long range alignment in the system. For systems with parallel alignment, i.e. all molecules having the same orientation and dipole moment direction, all three quantities converge to 1. In a perfectly disordered system all three are 0. A perfectly antiparallel dipolar alignment would also yield an S_1 value of 0. Thus S_1 alone is unable to discriminate between a disordered and an antiparallel state. On the other hand, a high value of S_2 can be attributed to either parallel or antiparallel orientation. By using the two parameters together one can distinguish between disordered, parallel and antiparallel states effectively. The S_4 order parameter can provide partial information about perpendicular ordering in the system: S_4 close to 1 indicates, but does not discriminate between, parallel and antiparallel alignment. Instead, S_4 tends towards a value of 0.6 in systems with both parallel and perpendicular alignment: note that in an extended system with full perpendicular organization, 50% of particles will lie in one direction (thus be parallel to each other), and the rest will lie along a perpendicular direction.

To quantify the degree to which molecules group in monolayer and multilayer structures, we calculated the fraction of molecules and the fraction of atoms which contact the surface. The molecule fraction is always lower than that of atoms, since at least one atom touches the surface when a molecule touches the surface, but is directly related to the definition of a monolayer or a multilayer. We report the fraction of molecules touching the surface in the following pages.

3 Results and Discussion

At the simplest level, surface SA represents the outcome of the coupling between inter-molecular and molecule-surface interactions. In one limit, the surface acts as mere support, with SA being dictated by the three-dimensional crystalline structure adopted by molecules in the absence of the surface. In the other limit, the substrate-molecule interaction can be so strong as to strongly impact the geometry of the monolayer. Between these two extremes, entirely new phases with varying degrees of order may become energetically favored. We examine these effects in the following sections.

3.1 Surface potential, dipole strength and order

Diatomic, dipolar molecules are a first-approximation model for self-assembling systems. The simplicity of the model allowed us to isolate steric (excluded-volume) effects, important in close-packed environments, from the effect of Coulombic interactions. We know that alkythiol self-assembly, for example, is greatly directed by the bulky alkyl group, from the organization of laying-down phases, to the tilt and phase behavior of upright monolayers. We will add some of that complexity later on, but first, what would the headgroup, or polar substituents like to do, if they were allowed to adsorb alone on the substrate?

The series of models A1-A3 are diatomic molecules with partially charged atoms. We considered partial charges ranging from almost neutral to high, and both strongly and weakly-attractive surface atoms (see Table 1). In these simple systems, the interplay between intermolecular and molecule-surface forces re-

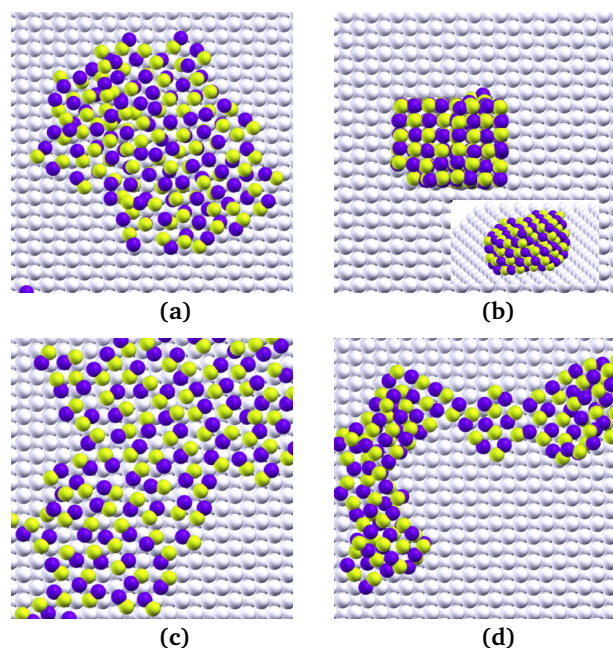


Fig. 2 Pattern formation in simple dipolar adsorbates. Snapshots of A-series molecules adsorbed on a surface with two different LJ energy parameters ϵ_{ss}^* are presented. Panels (a) and (b) show condensed phase snapshots for A1 and A3, respectively, when surface interaction is relatively weak ($\epsilon_{ss}^* = 1$). An insert in (b) shows a side view of the crystal. Panels (c) and (d) show snapshots for molecules A1 and A2, respectively, at $\epsilon_{ss}^* = 3$. Panels present replicas at $T^* = 0.1-0.2$.

sulted in structures spanning a range between surface-driven and intermolecular interactions-driven adsorption.

Strong lateral interactions dominated the self-assembly process, with small regard given to the surface attraction or geometry. In the case of molecule A3, for example, multi-layer crystalline structures were observed, similar to dipolar crystals formed in gas phase. At times, crystals formed above the surface without adsorption, particularly at higher temperatures. As shown in Figure 2(b), the multilayer structure exhibited sharp corners, indicative of a crystalline state. At the other extreme, weak intermolecular forces in systems with low polarity led to surface-directed patterning, where molecules commensurated with the surface to a degree determined by strength of the surface attraction. Figures 2(a) and (c), for example, show snapshots obtained for normal and strong surface attraction, respectively. In Figure 2 (c), in particular, molecules moved apart from van der Waals distances in order to commensurate with surface pit sites. This led to molecular axes aligned on [110] or [-110] directions, along the lines of pit sites, with large intermolecular distances. In the case of molecule A1, polarity was too weak to even enforce intermolecular alignment at the larger intermolecular distances. These effects were reflected in the values of order parameters for these systems (see Table 2).

In the intermediate regime, a competition of the two driving forces ensued. As shown in Table 2 for molecule A2, lateral interactions of intermediate strength did not necessarily enhance ordering over weakly interacting molecules. Stronger interactions biased the structures towards close-packed arrange-

Table 2 First, second and fourth order parameters S_1 , S_2 and S_4 .

Molecule	S_1	S_2	S_4
A1*	0.00	0.05	0.10
A1 [§]	0.00	0.18	0.31
A2*	-0.01	0.01	0.26
A2 [§]	0.00	0.17	0.28
A3	-0.01	0.03	0.50
C1-l	0.00	0.15	0.33
C2-l	0.00	0.10	0.28
C3-l	0.01	0.20	0.26
C4-l	0.02	0.23	0.25
C1-h	-0.01	0.01	0.24
C2-h	-0.01	0.00	0.03
C3-h	0.64	0.43	0.10
C4-h	0.75	0.58	0.23
D1	-0.01	0.01	0.24
D2	-0.01	0.01	0.03
D3	-0.01	0.10	0.08
D4	0.00	0.19	0.22
L1	-0.01	0.03	0.03
L2	0.00	0.23	0.24
L3	0.00	0.23	0.27
G1 ₁ -l [‡]	0.00	0.17	0.12
G1 ₂ -l	-0.01	0.27	0.36
G1 ₃ -l	0.06	0.31	0.37
G1 ₄ -l	0.04	0.29	0.35
G2 ₁ -l	0.00	0.12	0.03
G2 ₂ -l	0.00	0.13	0.01
G2 ₃ -l	0.17	0.18	0.07
G3 ₁ -l	0.01	0.12	0.10
G3 ₂ -l	0.04	0.08	0.15
G3 ₃ -l	0.12	0.05	0.12
G3 ₄ -l	0.13	0.05	0.11
G1 ₁ -h	-0.01	0.11	0.21
G2 ₁ -h	-0.01	0.01	0.04
G3 ₁ -h	0.00	0.03	0.08

S values for $\epsilon_{ss}^ = 1$ are shown here. [§]S values for $\epsilon_{ss}^* = 3$.

[‡]Parameters for biaxial molecules reported for the correlation of dipole axes. Order parameters for backbone axes are presented in the ESI Table 1[†].

ments, whereas surface-molecule interactions favored a more sparsely-spaced commensurate structure. The mismatch led to frustration in conditions of comparable lateral interactions and molecule-surface interactions. When a stronger surface potential was imposed, molecules A2 formed a commensurate monolayer, with dipolar alignment enforced by the molecules' stronger charge [see Figure 2(c)].

One note must be made at this point regarding the relationship between dipolar ordering and the values of the order parameters S_1 and S_2 : crystalline order does not necessarily lead to order parameters that are close to unity. As revealed by close examination of the highly ordered snapshots in Figures 2(b) and (d), pairs of molecules arranged in two types of relative orientations: the well-known antiparallel arrangement, and a perpendicular, "L-shaped" arrangement that also optimizes Coulombic interactions between

charges systems with more than 2 molecules.

At a given surface potential, simple diatomic dipolar molecules can thus be assembled in patterns ranging from partially ordered monolayers, to disordered multilayers, to aggregates and ordered crystalline structures by varying the intensity of the molecular dipoles (Figure 2). Many experimentally relevant systems have also been found somewhere between the two limiting cases of polarity-determined and surface-determined SA. Often times, organic molecules form SAMs by interacting strongly with the surface while having some geometric feature that directs how patterns are formed. For example, in two-dimensional arrays of 4-aminobenzoic acid on Cu(110), molecular positions were largely determined by the interaction between the surface and the benzene rings, and relative molecular orientations were determined by the molecular dipole moments.⁶¹ Conversely, surprising close-packed structures due to strong lateral interactions have been observed even at low coverage adsorption. For example, 2,4- and 2,6- dinitrotoluene formed close-packed domains on Au(111), with molecules aligned in parallel, surface-normal orientations, as a result of strong dipole-dipole and π -stacking interactions.⁶² In this case, the surface played only a secondary role, by immobilizing the layer. Beyond the simple dipole model, however, in most experimental SA studies, including the two mentioned here, steric (geometric) traits play important roles in determining SA outcomes. We explore below, with the use of series D, C, L and G, fundamental aspects of molecular geometry effects in surface SA.

3.2 Molecular length, dipole length, charges and order

In general terms, longer molecules experience enhanced parallelism due to van der Waals interactions between constituent atoms, as well as excluded volume effects. Long molecules can more efficiently pack in parallel configurations, a fact well understood through decades of liquid crystal research and needle-like models.^{63–65} The interplay between molecular length effects and dipole strength and length was examined here in some detail through series D, C and L.

3.2.1 Equal dipole moments, different molecular lengths.

The effects of a weakly interacting backbone in molecules with similar dipole moments were examined in models D1-4. Here, dipole length was increased by addition of spacer atoms, while holding constant the overall dipole moment by modifying end group charges accordingly (see Figure 1 and Table 1). Whereas the diatomic D1 molecules formed three-dimensional crystals [see Figure 3(a)], the behavior of the longer D2-4 molecules changed systematically, as longer molecules were driven to align parallel to the surface. The spacer groups served to enhance surface-molecule interactions, but also inhibited L-shaped alignment within the condensed phase. As a result, fairly disordered multilayer structures were observed in condensed phases of molecules D2 and to some extent D3 [Figure 3(b) and (c), respectively]. System-wide order was only observed again in assemblies of D4, where stronger molecule-surface interactions led to monolayer formation. Within the monolayer, molecules acquired antiparallel orientations, with the formation of connected domains. Here, adjacent antiparallel domains organized along

roughly perpendicular directions, as molecules aligned along the lines of surface hollow sites [e.g., Figure 3(d)].

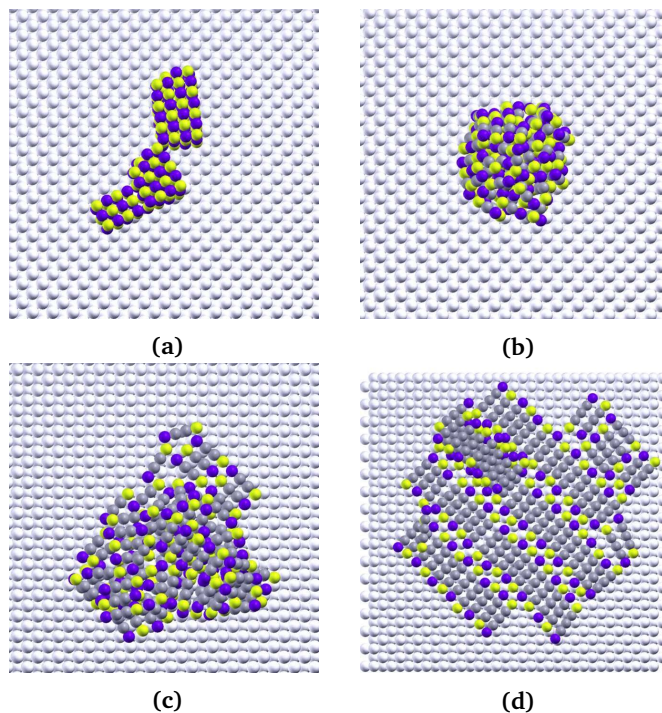


Fig. 3 Effects of molecular length on SA structure. Snapshots of dominant low-temperature phases corresponding to series D1 (panel a), D2 (panel b) and D3 (panel c), and an intermediate-temperature antiparallel phase for D4 (panel d) are presented.

These phase changes were reflected in the temperature dependence of the three order parameters: Figures 4(a)-(c) show decreased order at all temperatures in the shorter molecules D2 and D3, over D1 and D4. D4 molecules exhibited an apparent enhancement of their order parameter values around $T^*=3$. The increase paralleled an enhancement of monolayer character in the $T^*=2.5$ – 3.5 temperature range, where thermal energies became competitive with electrostatic interactions [see Figure 3(d)]. At lower temperatures, D4 molecules satisfied their electrostatic interactions by multilayer structures, where multiple molecules could bring their charges into contact more effectively. This was reflected in a lower fraction of molecules in contact with the surface at low temperatures [see Figure 4(d)]. On the other hand, standard deviations of the S_2 values for D4 were significant, as a result of the various packing arrangements of the antiparallel phase (as illustrated in the ESI Figure 2†), and the S_2 maximum at $T^*=3$ in Figure 4(b) is uncertain. A metastable nematic phase, discussed in the following section, further complicates the picture in these systems.

In a nutshell, the preferred tail-to-tail antiparallel configurations of dipolar systems can be disfavored in larger molecules, because of stronger surface-molecule interactions, and the need to match substrate geometries. However, in many cases, any series of molecules employed in surface SA experiments would have ever more complex geometries with binding substituents designed for a specific type of interactions, and that do not change in nature as the molecular backbone is increased. Such molecules

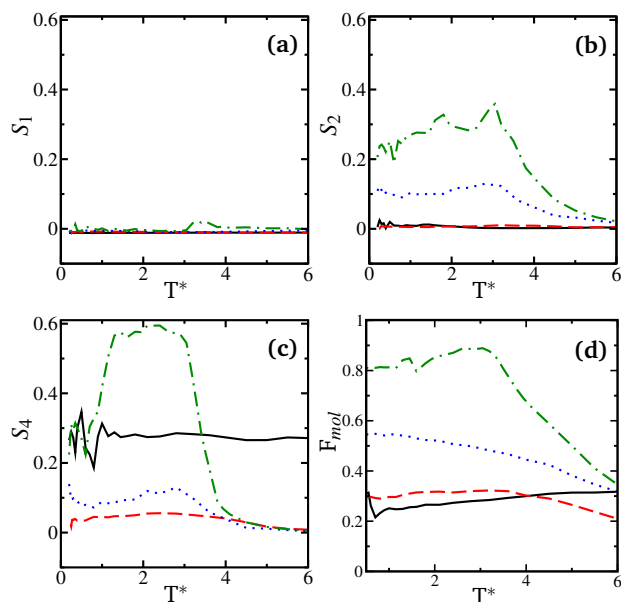


Fig. 4 Temperature dependence of order parameters in systems D. S_1 , S_2 and S_4 are shown in panels a-c, respectively. The fraction of molecules in contact with the surface is presented in panel d. Black lines, red dashes, blue dots and green dot-dashed lines represent systems D1-4, respectively.

often form highly ordered, stable monolayers, with defect-free phases extended over tens and hundreds of nanometers. We employed series C to examine these effects.

3.2.2 Equal partial charges, different molecular lengths.

We considered molecules of varying lengths with polar groups were located in similar, accessible locations, by using models C. Here, dipole length and dipole moment increased proportionally, as charges on end groups were held constant. Strongly and weakly polar molecules were examined using two sets of charges: series C-*h* had high charges similar to D1, so that C1-*h* and D1 were identical, while series C-*l* had lower charges, so that C4-*l* and D4 were identical (see Table 1).

The more polar series C-*h* exhibited a strong tendency towards the formation of three-dimensional crystalline structures, as lateral interactions overwhelmed surface-molecule attraction. C-*h* molecules generally formed multilayer structures to satisfy this preference [see ESI Figure 5(b)†], although longer molecules were more likely to have an extensive surface layer. C3-*h* and C4-*h* molecules were mostly lying parallel to the surface, with charged groups engaged in crystal-like stacking (see, for example, Figure 5). Unlike their D counterparts, molecular backbones in the C3-*h* and C4-*h* condensed phase structures were not aligned in tail-to-tail rows, but rather stacked like logs in a rail fence, allowing charged groups to interact with several opposite charges simultaneously, to the detriment of backbone dispersive interactions. Large values of S_1 and S_2 (Table 2), indicate that most molecular dipoles were pointing in the same direction in these systems.

The weakly-polar C-*l* analogues exhibited dramatically different temperature-dependent behavior (see Figure 6). Weaker elec-

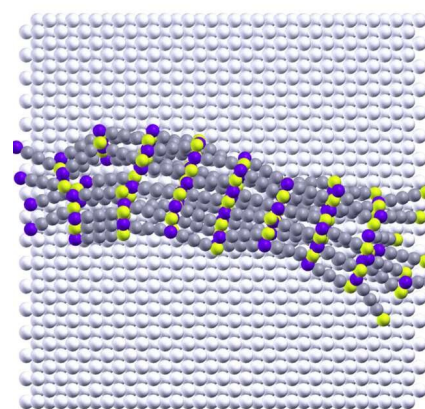


Fig. 5 Strong alignment for long, high-charge molecules. A low-temperature snapshot C4-*h* is shown

trostatic forces allowed for a mostly single-layer distribution of the molecules on the surface. Because of greater balance between electrostatic and dispersive contributions to the potential energy surface, a more complex phase behavior characterized systems C-*l*, as illustrated by the temperature dependence of the S_2 order parameter [Figure 6(a)]. Simple 2-D crystal ordering in the short C1-*l* molecule gave place to antiparallel domain formation upon addition of spacer atoms in C2-*l* and C3-*l* [see Figure 6(b)]. At higher temperatures, mainly antiparallel rows were observed [Figure 6(c)].

Entropic effects and lateral dispersive interactions in the long-backbone molecule C4-*l*/D4 led to two polymorphs in this system: a metastable nematic phase,⁶⁶⁻⁷⁰ found often at higher condensed-phase temperatures [Figure 6(d)], and the stable antiparallel-domains phase discussed in relation to Figure 3(d) above. Lengthy PTMC runs (over 5×10^{10} steps) eliminated completely the nematic phase, but its persistence throughout the simulation is worth noting. The presence of the two polymorphs (the nematic and antiparallel states), with distinct order parameters, led to a bimodal distribution for all of the order parameters for model C4-*l*/D4, and ill-defined averages for these parameters. This is illustrated at some length in the ESI Figures 2-4†: The figures provide a comparison between the fully converged D4 model (ESI Figure 2), the metastable C4-*l*/D4 polymorph (ESI Figure 3) and G12-*l* (ESI Figure 4). The latter did not exhibit polymorphic behavior. Whereas S_2 for G12-*l* showed a statistical spread around the 0.3 average at $T^* = 1.4$ and S_1 for the same system was 0, both order parameters oscillated around two distinct values in the case of the metastable C4-*l*/D4 (around 0 and 0.9 for S_1 , and around 0.2 and 0.9 for S_2). As the nematic state is not sampled at any temperature in the fully converged D4 system (see ESI Figure 2†), it appears that the state is kinetically trapped for the C4-*l*/D4 simulation.

Applications of surface functionalization can be based on a variety of patterning motifs, from two dimensional arrays, to surface-supported clusters, to the formation of independent, self-contained domains on the surface. For example, sensing applications may require organized surface-supported clusters, heterogeneous catalysis or device applications need extended, well-

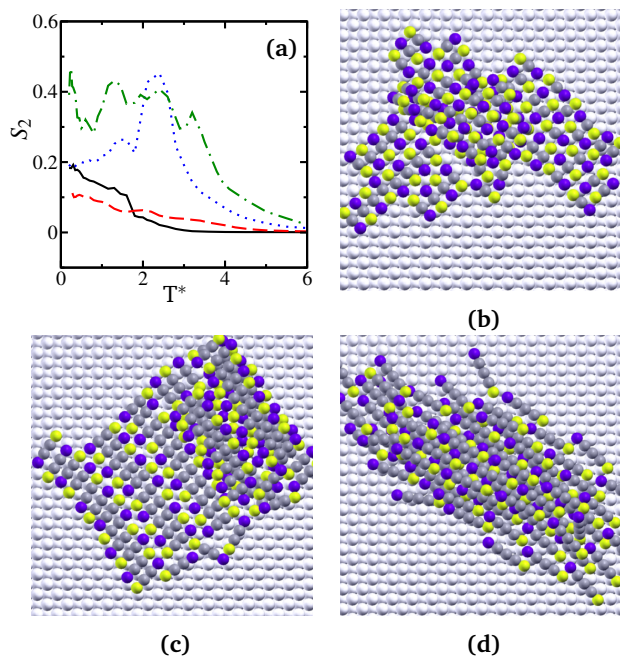


Fig. 6 Complex phase diagrams in low-charge systems. In (a), the temperature dependence of S_2 for systems C1-l, C2-l, C3-l and C4-l is shown with solid black, dashed red, dotted blue and dot-dashed green lines, respectively. A low temperature snapshot showing C2-l in antiparallel configuration is shown in (b). High ordering in antiparallel rows was observed for C3-l at intermediate temperatures - $T^*=2.5$ is shown in (c). An example of the medium temperature nematic phase at $T^*=2.5-3.5$ is given in (d) for C4-l/D4.

organized two-dimensional arrays of specific densities, while nanofabrication of molecular wires requires sufficiently separated neighboring wires.

In the latter case, molecules have to interact specifically in one direction while resisting interaction in the other directions. Positioning the partial charges on the outer atoms enables molecules to maximize dipole-dipole interaction by head-tail and lateral alignment. This ensures that a two-dimensional layer is preferred over one-dimensional domains. One way to partially restrict the dipole-dipole interaction to one direction is by embedding the partial charges within the molecule, with unreactive molecular ends.

3.2.3 Varying the molecular location of charged groups.

Embedded charge models were represented in the current study by series L (see Figure 1). The series comprised three molecular models, with equal length, equal dipole moment, but varying charges and charge separation. In model L1, charges were located in the middle of the molecule in neighboring positions, with relatively large dispersive groups on each side. Model L1 exhibited amphiphilic behavior at low-to-medium temperatures: clusters or chains, with charges grouped on the inside and bulky groups pushed to the outside can be seen in Figure 7(a). As side substituents decreased and eventually disappeared, models L2 and L3 formed mainly antiparallel structures, as shown in Figure 7(b). Moreover, the long, end-group-polarized L3 exhibited polymorphism similar to that discussed for D4, but with molecu-

lar rows in the nematic phase arranged in a standard tail-to-tail distribution [Figure 7(b) and (c)].

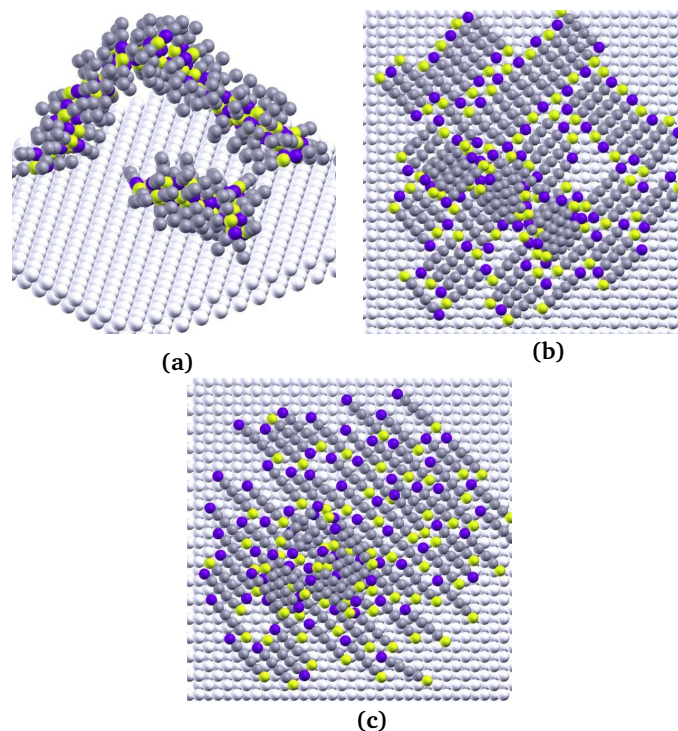


Fig. 7 The effects of relative positioning of charged atoms within molecules. Snapshots of simulations corresponding to models L1 at low to intermediate temperatures (a), L3 in its antiparallel phase (b), and L3 in a compact nematic - [panel (c)] configuration.

3.3 Asymmetry

Molecular asymmetry was introduced in series G by using bulky substituents and non-linearity. Both modifications were expected to interfere with the close-packed arrangements discussed above for linear molecules. Models G-h have a pair of strong partial charges and one bulky substituent, arranged at different angles versus the dipole direction. A low-charge series, G-l, was also considered, as were longer tailgroups of the lower-charge series. Beside geometric asymmetry, these models consider an additional aspect of asymmetry of the charge distribution: whereas models C, D and L presented oppositely charged atoms placed symmetrically within the molecule, models G have their charge distribution concentrated on one side of the molecule (a headgroup), with the other side being uncharged and exclusively dispersive (a tailgroup). As observed for symmetric models with strong charges (A, C-h), models G-h formed strongly crystalline structures. However, the presence of bulky groups in G-h impeded crystal growth in one or two directions, which resulted in the formation of crystalline wires, with bulky groups pushed towards the outside of the chain [see, for example, Figure 8(a)]. Similar results were obtained for G2-h and G3-h.

As charged groups were stacked in a variety of ways within these molecular wires, low values of the order parameters were observed, despite strong dipolar ordering in these systems. Sharper molecular angles were harder to accommodate in con-

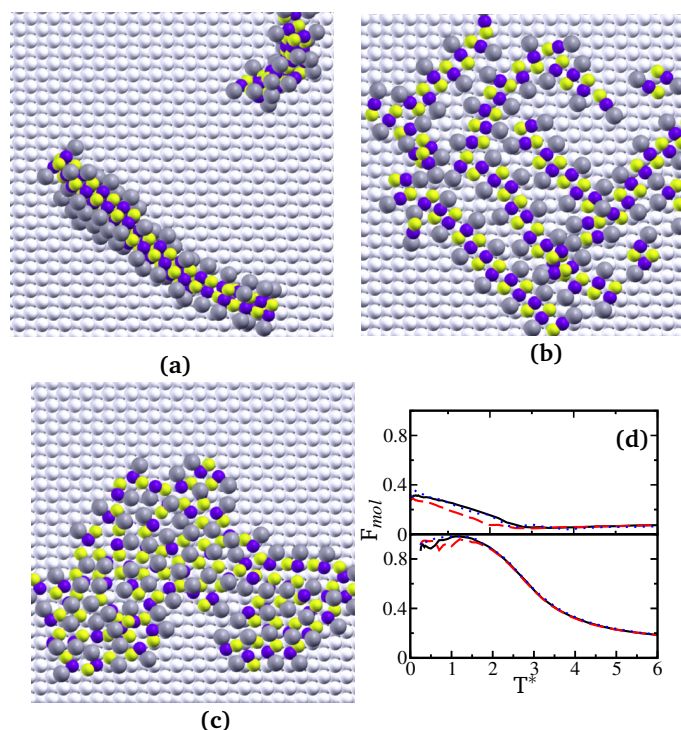


Fig. 8 The effect of asymmetry on self-assembled structures. Low-temperature snapshots from simulations corresponding to models $G1-h$, $G1-l$ and $G3-l$ are presented in panels a-c, respectively. The graph in panel d shows the fraction of molecules in contact with the surface for the $G-h$ series (above) and the $G-l$ series (below). Black solid lines, red dashes and blue dots correspond to systems $G1$, $G2$ and $G3$, respectively.

densed phases, leading to a relative loss of dipolar alignment in condensed phases of $G3-h$ and $-l$.

As before, weaker charges led to an increased dominance of surface-molecule interactions in the resulting structures. Chain-like structures in high-charge models became surface bound [see, for example, Figure 8(b) and (d)] in low-charge models, and monolayers exhibited atomic localization at pit surface sites, as observed previously for strongly-attractive surfaces. Figure 8(c) for example, shows how dipolar alignment and surface attraction can be reconciled in model $G3-l$, for example, by locating the bulky, uncharged atom above the dipolar plane.

In effect, the case presented in Figure 8(c) is one where the dipolar attraction overcame the surface-tailgroup interaction, leading to compact phases where the dipoles could interact with multiple neighbors. In contrast, molecule $G1-l$ had no opportunity to push its tailgroup out of the way and form compact dipolar structures, leading to the formation of planar antiparallel chains. A different situation arose when longer molecular backbones lead to stronger tail-tail and tail-surface interactions, and tailgroup-directed assembly. Systems G_N-l where $N = 2, 3, 4$ provide illustrations of tail-driven assembly. Figure 9 presents two systems where compact, planar arrangements of the tailgroups were the dominant feature, with dipolar interactions determining the relative arrangement of molecular rows (aligned or antiparallel). In long-tail systems with two distinct interaction directions, it was useful to quantify the alignment of the second relevant direction.

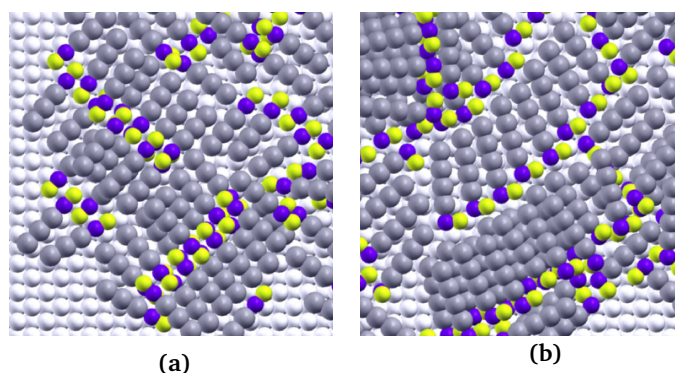


Fig. 9 Tail-driven assembly in asymmetric molecules. Low-temperature snapshots from simulations corresponding to models $G1-l$ and $G3-l$ are presented in panels a and b, respectively.

As shown in ESI Figures 6 and 7†, tailgroup alignment was more regular than dipolar alignment in systems with tailgroup-directed assembly (see also the dipole-based and tailgroup-based order parameter values presented Table 2 and ESI Table 1†, respectively).

Most molecules of interest to SA scientists are asymmetric in nature, often exhibiting distinct polar and apolar molecular regions. Despite more complex interaction patterns, similar effects have been observed in experimental studies seeking a fundamental understanding of the dipole/steric interplay in SA systems. For example, thiophenes substituted with long (C18) alkylamide groups adopted distinct alignment strategies depending on the binding location of the alkylamide group to the thiophene ring.⁴¹ The long alkyl chains, $\pi-\pi$ interactions, the availability of hydrogen bonds and the polarity of the amido group provided a strong blueprint for the formation of self-assembled structures on graphitic surfaces. However, the overall pattern changed significantly depending on the molecular polarity, modified by varying the binding location of the alkyl amide group on the thiophene ring. When the C18-amido group was bound at the position 2 of the thiophene ring, the alkyl backbone and the dipole moment were roughly perpendicular, as in our $G3-l$ and $G3-l$ models, whereas in the 3-substituted thiophene, the two entities were roughly collinear, in a fashion similar to the trends explored by our $G1-l$ models. The overall effect was that the 2-substituted thiophenes assembled in a head to tail packing with a parallel alignment, whereas 3-substituted ones adopted head-to-head packing and an antiparallel alignment, similar to those shown in Figure 9(b) and (a), respectively.

4 Conclusion

In the present work, we examined some of the basic molecular variables controlling the emergence of order from disordered phases in surface self-assembly, by following several simple molecular models. We found that although simple dipoles formed the expected crystalline structures at low temperatures, modulation by the surface interaction and substituent effects significantly altered adsorbed structures. Longer molecules experienced stronger (cumulative) surface attraction and tended to form monolayers with lateral alignment in parallel (nematic) or antiparallel configurations. Stronger molecular dipoles led to

multilayer aligned phases, in which many polar groups could be found in close vicinity. Limiting the availability of contact points by substituent effects, in addition to the steric effect of such apolar substituents further altered self-assembled structures, with the formation of molecular wires, stabilized on or off the surface by the relative strength of the interactions, in a number of cases.

Clearly, intermolecular interactions in experimental systems span a significantly broader range than those considered here, although, as shown in the current work, fundamental features can often be captured through simple models. We are currently studying structure formation in experimentally-relevant molecules such as substituted polar acenes, using a combination of classical PTMC and density functional theory. However, at the base of all types of supramolecular interactions lay fundamental electrostatic and geometric effects. The present work explored the wealth of self-assembled phases generated by their interplay and provided an understanding of how these effects can be exploited to alter molecular behavior upon adsorption. Further model-based studies will focus on the availability of multiple contact points, both between molecules and with the surface, as well as on solvent effects, bringing the complexity of the theoretical model closer to experimentally-relevant molecular systems.

5 Acknowledgement

Funding was provided by the National Science and Engineering Research Council of Canada, the Canada Foundation for Innovation, the British Columbia Knowledge Development Fund and the University of Victoria. This research was performed in part using the WestGrid computing resources, which are funded in part by the Canada Foundation for Innovation, Alberta Innovation and Science, BC Advanced Education, and the participating research institutions.

References

- 1 G. Whitesides, J. Mathias and C. Seto, *Science*, 1991, **254**, 1312–1319.
- 2 B. A. Grzybowski, C. E. Wilmer, J. Kim, K. P. Browne and K. J. M. Bishop, *Soft Matter*, 2009, **5**, 1110.
- 3 M. Grzelczak, J. Vermant, E. M. Furst and L. M. Liz-Marzan, *ACS Nano*, 2010, **4**, 3591–3605.
- 4 P. E. Laibinis and G. M. Whitesides, *J. Am. Chem. Soc.*, 1992, **114**, 9022–9028.
- 5 I. Felhosi, E. Kalman and P. Poczik, *Russian Journal of Electrochemistry*, 2002, **38**, 230–237.
- 6 B. Parviz, D. Ryan and G. Whitesides, *IEEE Transactions on Advanced Packaging*, 2003, **26**, 233–241.
- 7 P. Manandhar, J. Jang, G. C. Schatz, M. A. Ratner and S. Hong, *Phys. Rev. Lett.*, 2003, **90**, year.
- 8 K. A. Brown, D. J. Eichelsdoerfer, X. Liao, S. He and C. A. Mirkin, *Frontiers of Physics*, 2013, **9**, 385–397.
- 9 J. Liu, X. Zhang, G. Dong, Y. Liao, B. Wang, T. Zhang and F. Yi, *Applied Surface Science*, 2014, **289**, 300–305.
- 10 N. K. Chaki and K. Vijayamohan, *Biosensors and Bioelectronics*, 2002, **17**, 1–12.
- 11 V. Humblot, S. Barlow and R. Raval, *Progress in Surface Science*, 2004, **76**, 1–19.
- 12 L. Wang, H. Kong, X. Song, X. Liu and H. Wang, *Phys. Chem. Chem. Phys.*, 2010, **12**, 14682.
- 13 A. Ulman, *Chem. Rev.*, 1996, **96**, 1533.
- 14 L. Xu, X. Miao, X. Ying and W. Deng, *J. Phys. Chem. C*, 2012, **116**, 1061–1069.
- 15 C.-A. Palma, M. Cecchini and P. Samorì, *Chem. Soc. Rev.*, 2012, **41**, 3713.
- 16 G. M. Whitesides, *Science*, 2002, **295**, 2418–2421.
- 17 J. C. Love, L. A. Estroff, J. K. Kriebel, R. G. Nuzzo and G. M. Whitesides, *Chemical Reviews*, 2005, **105**, 1103–1170.
- 18 F. Schreiber, *Progress in Surface Science*, 2000, **65**, 151–257.
- 19 R. G. Nuzzo and D. L. Allara, *J. Am. Chem. Soc.*, 1983, **105**, 4481–4483.
- 20 P. Cyganik, M. Buck, T. Strunskus and A. Shaporenko, *J. Am. Chem. Soc.*, 2006, **128**, 13868–13878.
- 21 R. Desikan, S. Armel, H. M. M. III and T. Thundat, *Nanotechnology*, 2007, **18**, 424028.
- 22 G. M. Whitesides, J. K. Kriebel and J. C. Love, *Sci. Prog.*, 2005, **88**, 17–48.
- 23 H.-Y. Chang, C.-C. Huang, K.-Y. Lin, W.-L. Kao, H.-Y. Liao, Y.-W. You, J.-H. Lin, Y.-T. Kuo, D.-Y. Kuo and J.-J. Shyue, *J. Phys. Chem. C*, 2014, **118**, 14464–14470.
- 24 Y. Arima and H. Iwata, *Biomaterials*, 2007, **28**, 3074–3082.
- 25 G. B. Sigal, M. Mrksich and G. M. Whitesides, *J. Am. Chem. Soc.*, 1998, **120**, 3464–3473.
- 26 N. Afara, S. Omanovic and M. Asghari-Khiavi, *Thin Solid Films*, 2012, **522**, 381–389.
- 27 F. Meder, S. Kaur, L. Treccani and K. Rezwan, *Langmuir*, 2013, **29**, 12502–12510.
- 28 N. Gozlan and H. Haick, *J. Phys. Chem. C*, 2008, **112**, 12599–12601.
- 29 C.-H. Kuo, H.-Y. Chang, C.-P. Liu, S.-H. Lee, Y.-W. You and J.-J. Shyue, *Phys. Chem. Chem. Phys.*, 2011, **13**, 3649.
- 30 W.-C. Lin, S.-H. Lee, M. Karakachian, B.-Y. Yu, Y.-Y. Chen, Y.-C. Lin, C.-H. Kuo and J.-J. Shyue, *Phys. Chem. Chem. Phys.*, 2009, **11**, 6199.
- 31 E. Beurer, N. V. Venkataraman, M. Sommer and N. D. Spencer, *Langmuir*, 2012, **28**, 3159–3166.
- 32 R. K. Smith, P. A. Lewis and P. S. Weiss, *Progress in Surface Science*, 2004, **75**, 1–68.
- 33 M. Jaccob, G. Rajaraman and F. Totti, *Theoretical Chemistry Accounts*, 2012, **131**, year.
- 34 C.-H. Kuo, C.-P. Liu, S.-H. Lee, H.-Y. Chang, W.-C. Lin, Y.-W. You, H.-Y. Liao and J.-J. Shyue, *Phys. Chem. Chem. Phys.*, 2011, **13**, 15122.
- 35 S. R. Punireddi, I. Platzman, R. T. Tung and H. Haick, *J. Phys. Chem. C*, 2010, **114**, 18674–18678.
- 36 C. Gahl, R. Schmidt, D. Brete, E. R. McNellis, W. Freyer, R. Carley, K. Reuter and M. Weinelt, *J. Am. Chem. Soc.*, 2010, **132**, 1831–1838.
- 37 N. Heinemann, J. Grunau, T. Leißner, O. Andreyev, S. Kuhn, U. Jung, D. Zargarani, R. Herges, O. Magnussen and M. Bauer,

- Chemical Physics*, 2012, **402**, 22–28.
- 38 W. R. Browne and B. L. Feringa, *Annual Review of Physical Chemistry*, 2009, **60**, 407–428.
- 39 T. Weidner, F. Bretthauer, N. Ballav, H. Motschmann, H. Orendi, C. Bruhn, U. Siemeling and M. Zharnikov, *Langmuir*, 2008, **24**, 11691.
- 40 G. Pace, V. Ferri, C. Grave, M. Elbing, C. von Hanisch, M. Zharnikov, M. Mayor, M. A. Rampi and P. Samori, *Proc. Natl. Acad. Sci.*, 2007, **104**, 9937.
- 41 L. E. Heller, J. Whitleigh, D. F. Roth, E. M. Oherlein, F. R. Lucci, K. J. Kolonko and K. E. Plass, *Langmuir*, 2012, **28**, 14855–14859.
- 42 J. Puigmarti-Luis, A. Minoia, H. Uji-i, C. Rovira, J. Cornil, S. D. Feyter, R. Lazzaroni and D. B. Amabilino, *J. Am. Chem. Soc.*, 2006, **128**, 12602–12603.
- 43 Q. Chen, C. Perry, B. Frederick, P. Murray, S. Haq and N. Richardson, *Surface Science*, 2000, **446**, 63–75.
- 44 G. Tomba, M. Stengel, W.-D. Schneider, A. Baldereschi and A. D. Vita, *ACS Nano*, 2010, **4**, 7545–7551.
- 45 F. Ciccoira, J. A. Miwa, D. F. Perepichka and F. Rosei, *J. Phys. Chem. A*, 2007, **111**, 12674–12678.
- 46 M. Pivetta, M.-C. Blum, F. Patthey and W.-D. Schneider, *Angewandte Chemie International Edition*, 2008, **47**, 1076–1079.
- 47 M. Pivetta, M.-C. Blum, F. Patthey and W.-D. Schneider, *J. Phys. Chem. C*, 2009, **113**, 4578.
- 48 J.-M. Lehn, *Angewandte Chemie International Edition*, 2013, **52**, 2836–2850.
- 49 R. Gutzler, L. Cardenas and F. Rosei, *Adv. Mat.*, 2013, **25**, 449.
- 50 F. Zerbetto, *Adv. Mat.*, 2013, **25**, 449.
- 51 R. Gutzler, L. Cardenas and F. Rosei, *Chemical Science*, 2011, **2**, 2290.
- 52 G. Ercolani, *J. Am. Chem. Soc.*, 2003, **125**, 16097–16103.
- 53 C. A. Hunter and H. L. Anderson, *Angewandte Chemie International Edition*, 2009, **48**, 7488–7499.
- 54 C. Chapman and I. Paci, *J. Phys. Chem. C*, 2010, **114**, 20556–20563.
- 55 I. Paci, I. Szleifer and M. A. Ratner, *J. Phys. Chem. B*, 2005, **109**, 12935–12945.
- 56 D. Frenkel and B. Smit, *Understanding Molecular Simulation From Algorithms to Applications*, Academic Press, San Diego, California, 2002.
- 57 A. P. Lyubartsev, A. A. Martsinovski, S. V. Shevkunov and P. N. Vorontsov-Velyaminov, *J. Chem. Phys.*, 1992, **96**, 1776.
- 58 U. H. Hansmann, *Chemical Physics Letters*, 1997, **281**, 140–150.
- 59 W. L. Jorgensen, J. D. Madura and C. J. Swenson, *J. Am. Chem. Soc.*, 1984, **106**, 6638–6646.
- 60 T. Popa and I. Paci, *Chem. Phys. Lett.*, 2011, **507**, 128 – 133.
- 61 Q. Chen, D. J. Frankel and N. V. Richardson, *Surface and Interface Analysis*, 2001, **32**, 43–48.
- 62 H. Li, X. Jiang and B. G. Willis, *J. Phys. Chem. C*, 2014, **118**, 14418–14426.
- 63 H. Kraack, B. M. Ocko, P. S. Pershan, E. Sloutskin and M. Deutsch, *Science*, 2002, **298**, 1404–1407.
- 64 K. Morishige, N. Kawai and M. Shimizu, *Phys. Rev. Lett.*, 1993, **70**, 3904–3906.
- 65 J. C. Armas-Pérez and J. Quintana-H., *Physical Review E*, 2011, **83**, year.
- 66 J. M. Kosterlitz and D. J. Thouless, *J. Phys. C: Solid State Phys.*, 1973, **6**, 1181–1203.
- 67 J. A. Martínez-González, J. C. Armas-Pérez and J. Quintana-H., *Journal of Statistical Physics*, 2013, **150**, 559–571.
- 68 S. Varga, P. Gurin, J. C. Armas-Perez and J. Quintana-H., *The Journal of Chemical Physics*, 2009, **131**, 184901.
- 69 M. A. Bates and D. Frenkel, *The Journal of Chemical Physics*, 2000, **112**, 10034.
- 70 R. Tavarone, P. Charbonneau and H. Stark, *The Journal of Chemical Physics*, 2015, **143**, 114505.